crystals

MDPI

Article

Effect of UV Irradiation on the Alternating Wet and Dry Corrosion Behavior of Galvanized Steel in Sodium Chloride Solution

Jilin Pan [1], Yuhao Wang [2], Liang Yang [2], Weiguang Li [1], Dan Yang [2], Baojie Dou [2,3,*], Chun Hu [2] and Xiuzhou Lin [2,3,*]

[1] Sichuan Chengdu Soil Environmental Materials Corrosion National Observation and Research Station, Chengdu 610062, China; panjilin@126.com (J.P.)
[2] School of Materials Science and Engineering, Sichuan University of Science & Engineering, Zigong 643000, China
[3] Material Corrosion and Protection Key Laboratory of Sichuan Province, Sichuan University of Science & Engineering, Zigong 643000, China
* Correspondence: baojiedou@suse.edu.cn (B.D.); linxiuzhou@suse.edu.cn (X.L.)

Abstract: In this paper, the corrosion performance of galvanized steel was investigated in a simulated marine environment, under UV irradiation coupling with an alternating wet and dry cycle in a NaCl solution. The surface morphology, composition, and corrosion performance of galvanized steel before and after different alternating wet and dry corrosion under UV irradiation were investigated. The results show that the corrosion current density gradually increases and the corrosion resistance decreases as a function of the alternating wet and dry corrosion cycles. Meanwhile, UV irradiation accelerates the increase in the corrosion current density and the decrease in the corrosion resistance. In addition, the corrosion product ZnO shows a semiconductor property, and the photo-induced electrons and holes produced under UV can participate in the corrosion reaction and promote the formation of loose corrosion products $Zn(OH)_2$, $Zn_5(OH)_8Cl_2$, and $Al_2Cl_3(OH)_5{\cdot}4H_2O$, thus accelerating the corrosion of galvanized steel in the atmosphere environment.

Keywords: marine environment; temperature; ultraviolet radiation; wet/dry alternation; hot-dip galvanized steel

check for updates

Citation: Pan, J.; Wang, Y.; Yang, L.; Li, W.; Yang, D.; Dou, B.; Hu, C.; Lin, X. Effect of UV Irradiation on the Alternating Wet and Dry Corrosion Behavior of Galvanized Steel in Sodium Chloride Solution. *Crystals* **2023**, *13*, 1195. https://doi.org/10.3390/cryst13081195

Academic Editor: Petros Koutsoukos

Received: 30 June 2023
Revised: 24 July 2023
Accepted: 28 July 2023
Published: 1 August 2023

Copyright: © 2023 by the authors. Licensee MDPI, Basel, Switzerland. This article is an open access article distributed under the terms and conditions of the Creative Commons Attribution (CC BY) license (https://creativecommons.org/licenses/by/4.0/).

1. Introduction

The marine environment is rich in resources, and the exploitation of the sea has become a hot topic. However, offshore equipment is extremely vulnerable to corrosion damage due to the complexity of the marine environment. Apart from the chloride corrosion, the equipment normally bears marine atmospheric corrosion under light radiation, splash, and wave-induced alternating wet and dry action, as well as wind, rain, waves, and currents of mechanical impact [1]. Galvanized steel is widely used in offshore vessels, oil rigs, island equipment, sewage pipes, and cross-sea bridges due to its high strength and low cost [2–5]. Therefore, the investigation of the effect of marine environmental factors on galvanized steel plays an important role in evaluating the service life of equipment in the marine environment.

Atmospheric corrosion is essentially an electrochemical corrosion process of materials in the dry/wet cycle under a thin electrolyte layer, variation of temperature, relative humidity (RH), rainfall, salt particles, and frequency of wet/dry cycling [6–8]. In the last few decades, many efforts have declared that temperature and RH have a significant effect on the corrosion performance of metal via variations in the physical and chemical state of the atmosphere/metal interface layer [9–12]. The salt particles in the air form droplets or electrolyte layers on the metal surface, formed when the temperature drops and RH rises. However, the droplets or the thickness of electrolyte layers decrease when

the temperature rises and the RH drops [11]. According to Fick's law, variations in the thickness of electrolyte layers affect the dissolution and diffusion of oxygen, resulting in different corrosion kinetics of metals [13]. The investigation demonstrated the corrosion rate under a thin electrolyte layer was much higher than that of the sample immersed in the solution, because of the accelerated dissolution and diffusion of oxygen in the thin electrolyte layer [14,15]. Meanwhile, the effect of temperature on the corrosion behavior of low-alloy steel in the marine atmosphere shows that the increase in temperature not only promotes the transport of aggressive ions Cl^- and the formation of local corrosion but also affects the solubility of oxygen gas in the thin electrolyte layer [12].

UV irradiation is also an indispensable factor affecting the corrosion of metal in the atmosphere corrosion when the metals are exposed to sunlight; the 2% ultraviolet (UV) in sunlight has a critical effect [16]. Many studies have confirmed that UV irradiation can affect the corrosion process of metals in the atmosphere. Song et al. [17] found that UV irradiation significantly increased the atmospheric corrosion rate and the positive optical voltage of carbon steel when they investigated the influence of UV irradiation on the atmospheric corrosion of Q235 carbon steel induced by NaCl. Liu et al. [18] also found the corrosion rate of carbon steel increased with the increase in temperature from 30 to 60 centigrade in the high-humidity tropical marine atmosphere. The effect of UV illumination on carbon steel was closely related to environmental temperature; the higher the environmental temperature, the greater the impact. A combination of electrochemical and spectroscopic techniques was built to study the corrosion behavior of Cu-Sn-pb ternary bronze under UV light; the results indicated that UV/visible illumination had a significant effect on the corrosion behavior of bronze covered with oxide films, and that visible light irradiation accelerated the dissolution rate of Cu and Pb and promoted the growth of corrosion layers on the bronze surface [16]. The study of the photoelectric cathodic protection performance of a coating system on stainless steel suggests that it has some corrosion protection after exposure to UV light [19]. TiO_2-coated steel revealed the corrosion rate increased due to the active oxygen generated by photoelectrochemical reaction under UV light [20]. The effect of UV irradiation on the corrosion of zinc was also investigated. Results show that UV irradiation apparently affected the atmospheric corrosion morphology and corrosion rate of zinc. Moreover, the corrosion products have a semiconductor property: the photo-induced electrons and holes produced under UV light which can participate in the corrosion reaction and affect the atmospheric corrosion rate of zinc [21–23].

Although the effect of UV on zinc and steel has been investigated, the investigation of the UV effect on galvanized steel is still very limited. The chemical composition and microstructures of galvanized steel are different from zinc and steel. The galvanization process with a molten 0.1–1 at% Al-Zn bath results in an outer layer (Zn-Al coating) and an intermetallic film in the form of Fe_2Al_5 Znx ($0 < x < 1$). Therefore, the degradation behavior of galvanized steel in wet/dry alternating corrosion environments with UV irradiation might be different. For this purpose, a wet/dry alternating corrosion test system coupled with UV irradiation was built to evaluate the degradation process of galvanized steel in a simulated marine atmosphere environment. The effect of UV irradiation on the variation of structure, composition, and corrosion electrochemical behavior of galvanized steel was systematically studied.

2. Materials and Methods

2.1. Materials

A commercial hot-dip Q345B galvanized steel was supplied by Shanghai Casting Enterprise Industrial Co., Ltd., Shanghai, China. The galvanized steel was cut into specimens measuring 45 mm × 35 mm × 5 mm using a wire cutter, and then a 3 mm hole was perforated in the middle of one side (as shown in Figure S1a). The specimens were degreased with acetone, rinsed with deionized water, and dried in cold air.

2.2. Alternating Corrosion Test System

Based on the temperature, humidity, and heat test chamber, a dry and wet alternating corrosion test system coupled with UV irradiation was built to simulate the dry and wet alternating corrosion state of galvanized steel in the marine environment, as shown in Figure 1. The corrosion medium was 3.5 wt.% NaCl solution, the test temperature was 45 ± 1 °C, the dry and wet ratio was 1:1 (1 cycle was 4 h, recorded as 1 T), the wet treatment was full immersion, the distance between the UV and the sample was 600 mm, and the dry treatment was placed under UV irradiation at a 250 mm distance. The UV irradiation was provided by a 15 W quartz UV lamp, a UV spectral range of 200–330 nm, and the UV irradiation intensity on the sample surface was 0.11 mV/cm^{-2}.

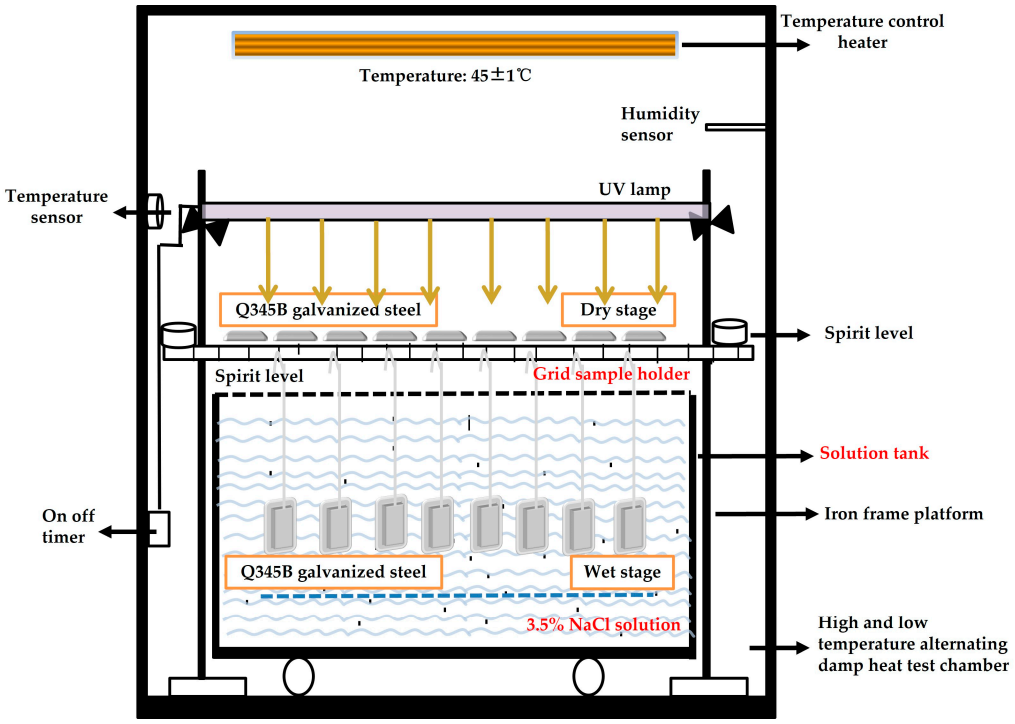


Figure 1. Schematic diagram of the wet/dry alternating corrosion test system.

2.3. Characterization

Potentiodynamic polarization curves (PDP) and electrochemical impedance spectroscopy (EIS) were used to evaluate the corrosion performance of the galvanized steel by an electrochemical workstation (CHI660D, Wuhan, China), with a conventional three-electrode cell, platinum plate as the counter electrode, a saturated calomel electrode (SCE) as the reference electrode, and the galvanized steel as the working electrode. Before the testing, the corrosion test system was left to stand for 30 min, and the open circuit potential (OCP) was recorded for 600 s. The PDP test ranged from −0.3 V vs. OCP to 1.5 V vs. SCE, and the scanning rate was 1 mV/s. EIS test was performed at frequencies ranging from 100 kHz to 10 mHz by using a 10 mV amplitude sinusoidal voltage at OCP. The data were fitted using ZSimpWin3.5 software. The PDP and EIS measurements were carried out three times to ensure the repeatability of the measurements.

The morphology of the galvanized steels before and after different dry and wet alternating corrosion tests were characterized by scanning electron microscopy (SEM, S4800, Hitachi, Tokyo, Japan) with an energy dispersive spectroscopy (EDS, X-MaxN, Oxford, UK). The crystalline structure of the samples was investigated by X-ray diffraction (XRD, D8 ADVANCE, BRUKER, Ettlingen, Germany) with Cu-Kα radiation (λ = 0.15406 nm).

3. Results

3.1. Electrochemical Behaviors

Potentiodynamic polarization measurement has been widely used to evaluate the anti-corrosion performances of metal and coated metals [24,25]. Figure 2 shows the potentiodynamic polarization curves of galvanized steel after different cycles of alternating wet/dry corrosion with and without UV irradiation. After different cycles of corrosion, the corrosion potential of the specimens under UV irradiation was more negative and the corrosion current density was also greater, indicating that the galvanized steel was much easier to corrode under UV irradiation than that of the samples without UV irradiation. Meanwhile, it is clearly revealed that the corrosion of galvanized steel under UV is much more serious than that of galvanized steel without UV, as shown in the polarization curves of the sample with and without UV in the same cycles of corrosion (Figure S2).

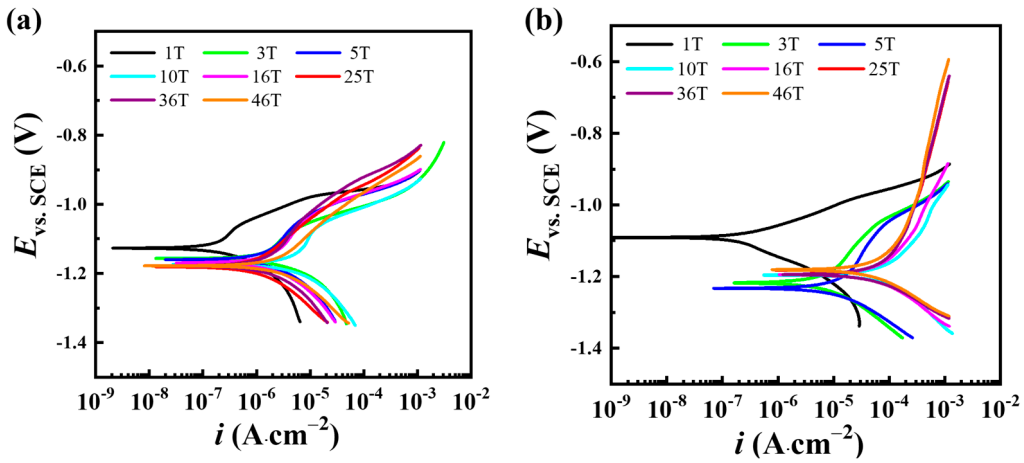


Figure 2. Polarization curves of galvanized steel after different cycles of corrosion in 3.5% wt.% NaCl solution (**a**) without UV; (**b**) with UV.

In order to compare the corrosion rate of galvanized steel, the corrosion potential (E_{corr}) and corrosion current density (i_{corr}) were calculated from the polarization curves, as shown in Figure 3. From Figure 3a, the corrosion potential of the galvanized steel without UV decreased dramatically and reached a stable value with the increase in the cycles of corrosion. The corrosion potential of the specimen under UV shows a trend of first decreasing and then gradually increasing with the increase in the cycles, reaching a minimum value of −1.233 V at 5 T. The corrosion potential of the specimens under UV irradiation is more negative than that without UV irradiation. One interpretation is, in the atmosphere environment, zinc can form ZnO, which has a typical semiconductor property that can promote the formation of photoelectrons and migration to the surface of the galvanized steel resulting in a shift of corrosion potential to a negative direction under UV. Generally, the more negative the corrosion potential, the more prone the metal is to corrode [26]. Therefore, galvanized steel is easier to corrode under UV irradiation than the samples without UV. Figure 3b shows the corrosion current density of the specimen with and without UV irradiation. As for the sample without UV, the corrosion current density increased from 2.24×10^{-7} A·cm^{-2} to the maximum of 6.23×10^{-6} A·cm^{-2} after 10 T cycles of corrosion; however, the corrosion current density of the specimen with UV irradiation increased from 2.22×10^{-7} A·cm^{-2} to the maximum of 5.76×10^{-5} A·cm^{-2} after 10 T cycles of corrosion and kept at approximately 5.00×10^{-5} A·cm^{-2} after 10 T cycles of corrosion. The corrosion current density of the specimen with UV irradiation was larger than that without UV irradiation. As described in a previous study, photoelectrons promote the generation of active oxygen to increase the corrosion of galvanized steel, resulting in a high corrosion current density under UV [20]. Figure S3 shows the Mott–Schottky (M-S) of the galvanized steels after different cycles of corrosion. After 1 T cycle of

corrosion, galvanized steels with and without UV show a typical positive slope, indicating that both surface samples are n-type semiconductors. The sample without UV shows a similar semiconductor property from 1 T to 10 T, but the semiconductor property of the sample gradually decreased after 16 T, which might be attributed to an increase in corrosion resulting in zinc oxide conversion to zinc hydroxide. However, the semiconductor property of the galvanized steels with UV declines or even disappears after 3 T cycle corrosion. Under UV, ZnO on the surface of galvanized steel will prove that the formation of photo-induced electrons and holes participate in the corrosion reaction and then promote the formation of loose corrosion products, such as $Zn(OH)_2$, $Zn_5(OH)_8Cl_2$, $Al_2Cl_3(OH)_5{\cdot}4H_2O$, which accelerate the corrosion of galvanized steel. From the above analysis, UV irradiation will accelerate the corrosion process of galvanized steel in a simulated marine atmosphere.

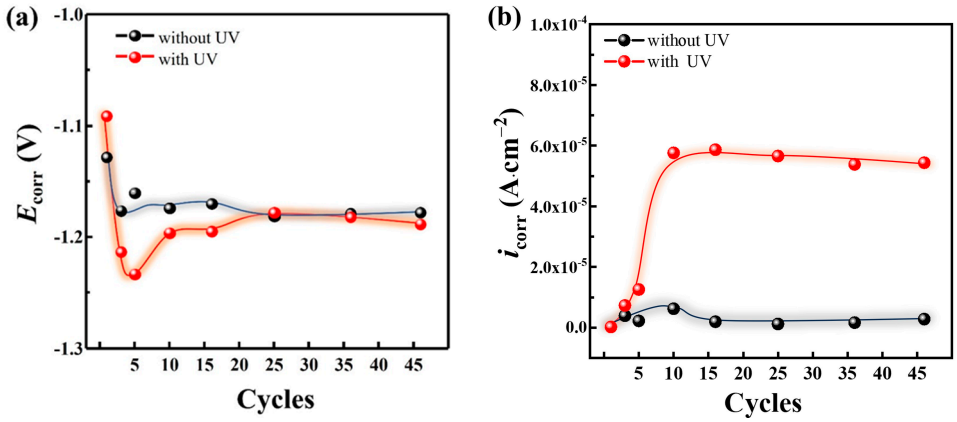


Figure 3. (**a**) Corrosion potential and (**b**) corrosion current density of galvanized steel after different cycles of corrosion in 3.5% wt.% NaCl solution with and without UV, and the total corrosion time is 180 h.

EIS was employed to evaluate the corrosion resistance and analyze the anti-corrosion mechanism of galvanized steel. Figures 4 and 5 show the EIS curves of galvanized steel after different cycles of corrosion with and without UV. As shown in Figure 4a, the impedance modulus of galvanized steel without UV decreased gradually with the increase in cycles of immersion, and the capacitive arc gradually decreased, as shown in Figure 4b, indicating the corrosion resistance of galvanized steel decreased as a function of the corrosion cycles. Meanwhile, there are two-time constants appearing, which were attributed to the zinc coating and the electrochemical corrosion reaction at the solution/zinc coating interface. The EIS data can be demonstrated by a physical model shown in Figure 6. R_s is the solution resistance; R_c and Q_c are the coating resistance and capacitance, respectively; and R_{ct} and Q_{dl} are the charge transfer resistance and capacitance, respectively [27]. From Figure 4c, as for the sample with UV, the impedance modulus of galvanized steel decreased dramatically from 10^4 Ω·cm^2 at 1 T to 1.81 × 10^4 Ω·cm^2 at 3 T and decreased with the increase in the cycles of immersion. The capacitive arc shifted to low frequency, suggesting the composition of the corroded galvanized steel has a significant change due to some special reaction occurring under UV.

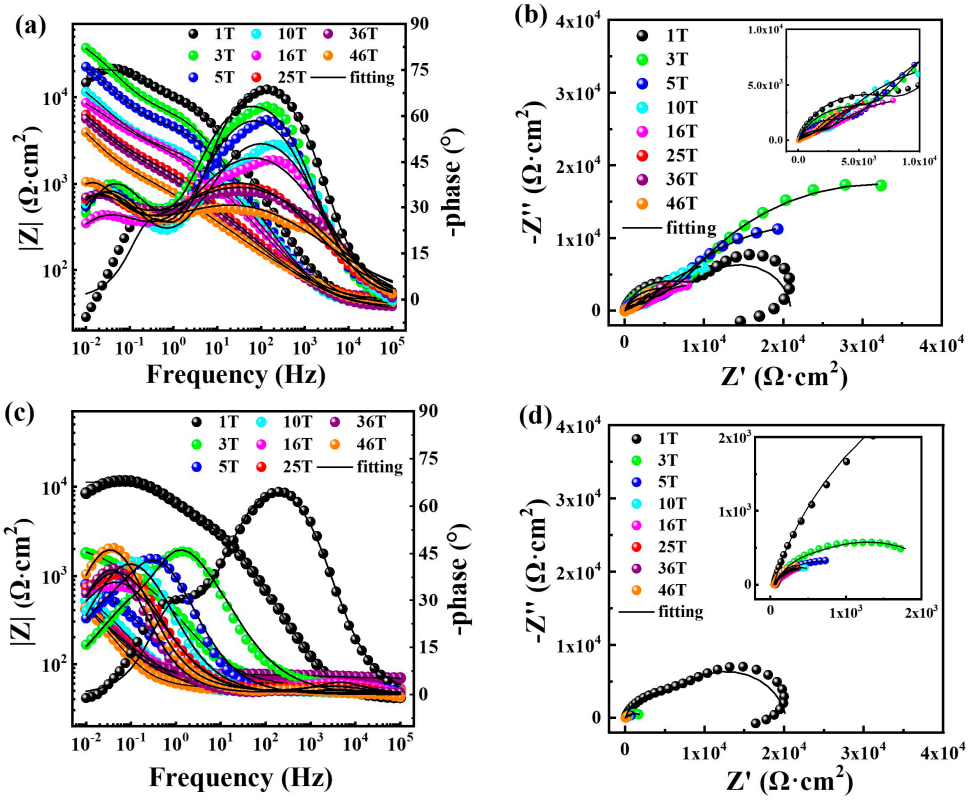


Figure 4. EIS curves of galvanized steel after different cycles of corrosion in 3.5% wt.% NaCl solution (**a**,**b**) without UV and (**c**,**d**) with UV.

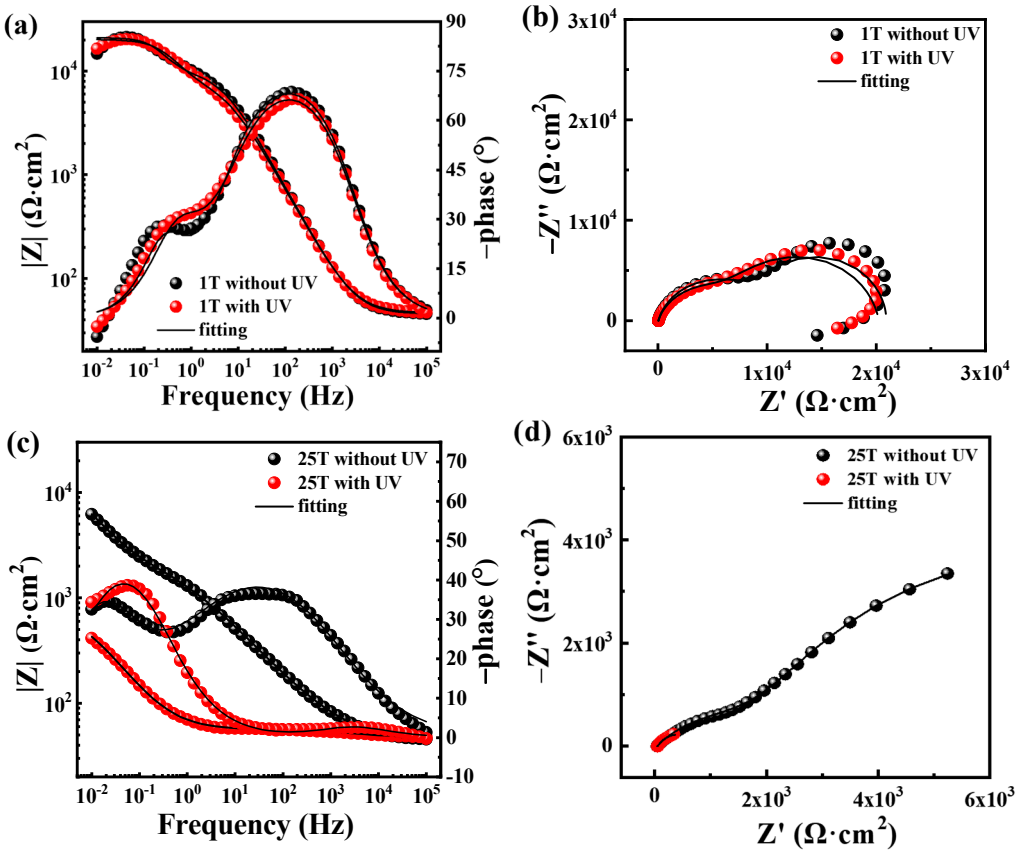


Figure 5. *Cont.*

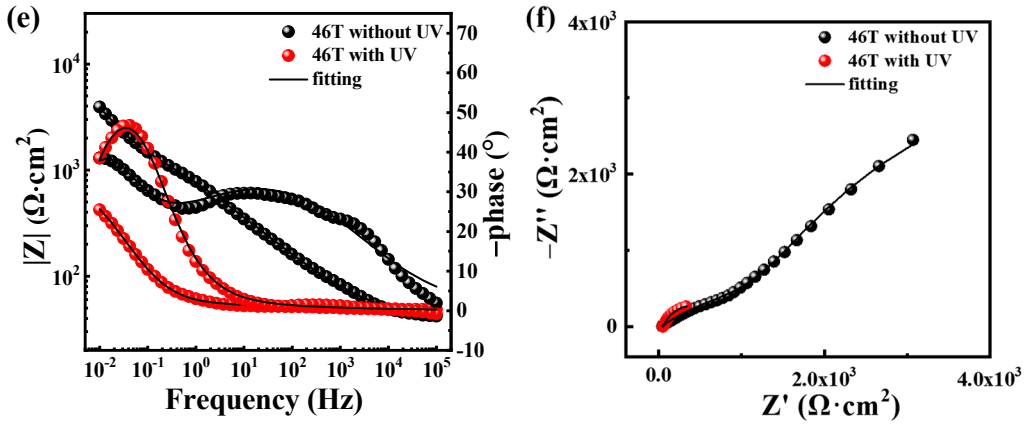


Figure 5. EIS curves of galvanized steel after different cycles of corrosion in 3.5% wt.% NaCl solution without and with UV (**a**,**b**) 1 T, (**c**,**d**) 25 T, and (**e**,**f**) 46 T.

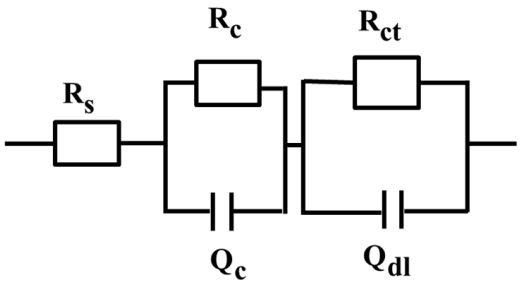


Figure 6. Fitting equivalent circuit model of electrochemical impedance spectroscopy.

Figure 5 shows a comparison of the EIS curves with and without UV for the same corrosion cycle. The EIS curves with and without UV at cycle 1 T are very similar; however, with the extension of the corrosion cycle, the EIS curves change significantly and the impedance modulus at 0.01 Hz decreases sharply with UV, indicating that UV exacerbates the damage to the galvanized coating, leading to a sharp reduction in corrosion resistance. Meanwhile, the phase constant in the plots of the galvanized steel shift to a low frequency, suggesting the composition of the galvanized steel has a significant difference under UV. This result should be attributed to the formation of ZnO with the semiconductor property, which changes the reaction on galvanized steel under UV. The composition of the corrosion products on galvanized steel will be detected by XRD to further verify the reaction.

In order to analyze the anti-corrosion mechanism of galvanized steel, this study used the equivalent circuit model (Figure 6) to fit the impedance data. Figure 7 shows the R_{ct} and R_c of galvanized steel after different cycles of corrosion in 3.5 wt.% NaCl solution without and with UV. R_{ct}, which is inversely proportional to corrosion rate, is a parameter representing the resistance of the electron transfer across the metal surface. The higher R_{ct} is, the more difficult the corrosion reaction, and hence the lower the corrosion rate [25]. As shown in Figure 7a, the R_{ct} values of galvanized steel without UV are higher than the samples with UV. The results indicate that UV accelerates the electron transfer on the surface of galvanized steel, and then increases the corrosion rate of galvanized steel.

R_c can be used as the parameter to reflect the barrier property of zinc coating to corrosive agents [28]. It can be found in Figure 7b that the R_c value of galvanized steel without UV is much higher than the sample with UV before 5 T corrosion cycle, and the R_c value decreased dramatically, indicating that the zinc coating has a good barrier property to corrosive agents at the beginning, but this decreases due to the corrosion reaction that occurred on the coating. Polarization and EIS data suggest that UV will affect the corrosion reaction on galvanized steel and accelerate the corrosion rate. Using SEM and XRD, we further analyze the structure and composition of galvanized steel in the different corrosion cycles.

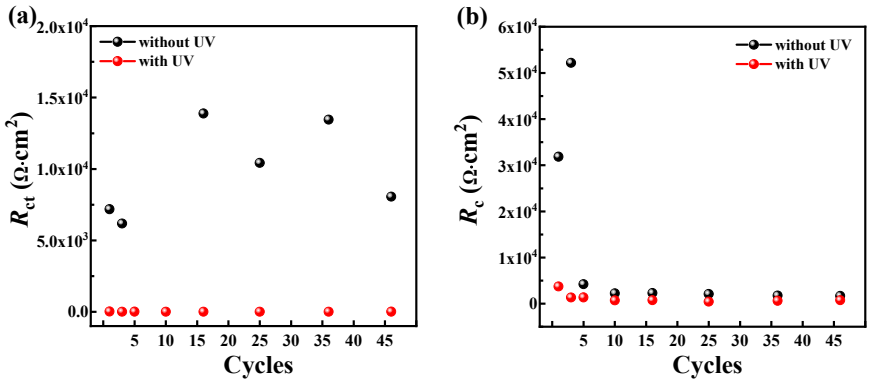


Figure 7. (**a**) R_{ct} and (**b**) R_c of galvanized steel after different cycles of corrosion in 3.5% wt.% NaCl solution without and with UV.

3.2. Structure and Composition

The corrosion morphology of the galvanized steel after different cycles was further analyzed using SEM and EDS; the results are shown in Figure 8 and Table 1. From Figure 8, the corrosion products on the surface of the galvanized steel with and without UV increased with the increase in corrosion cycles. Meanwhile, the corrosion products on the surface of the galvanized steel with UV was much more than that of the samples without UV after 1 T, 10 T, and 25 T. For 46 T, the corrosion products on the surface of the galvanized steel with UV were looser than those of the sample without UV, but it is difficult to distinguish the number of corrosion products. Therefore, EDS was performed on the galvanized steel after the 46 T experiment. Most of the corrosion products on the sample without UV were Zn and 12.87% O, indicating the corrosion products mainly might be oxide and hydroxide compounds. However, 28.47% O was detected on the surface of the galvanized steel with UV, suggesting much more zinc oxide and zinc hydroxide were formed. Meanwhile, 12.89% Cl elements were also detected, indicating the corrosion of galvanized steel with UV is more serious than that of the sample without UV, and new corrosion products might form under UV. These results indicated that UV irradiation not only accelerated the corrosion of galvanized steel, but also changed the corrosion process of galvanized steel, and the composition of corrosion products changed significantly. XRD was used to further analyze the structure of corrosion products to illustrate the degradation mechanism of galvanized steel under UV.

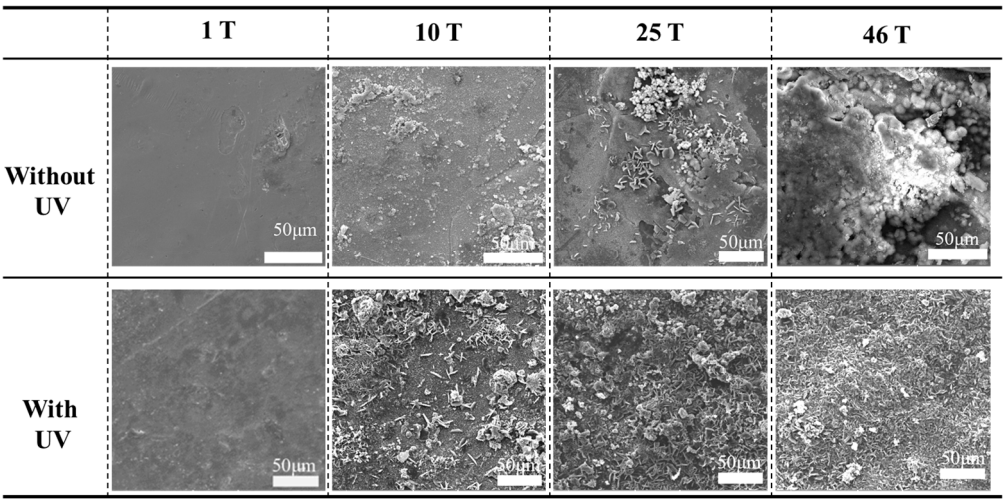


Figure 8. SEM of galvanized steel after immersion in 3.5% wt.% NaCl solution without and with UV for 1 T, 10 T, 25 T, and 46 T.

Table 1. Results of EDS analysis of galvanized steel after immersion in 3.5% wt.% NaCl solution with and without UV for 46 T.

Elements (W%)	Zn	O	Cl	Al	Other
Without UV	86.52	12.87	0.13	0.45	0.03
With UV	58.43	28.47	12.89	0.04	0.17

The composition of the corrosion products on galvanized steel was characterized using XRD. As shown in Figure 9, as for the galvanized steel without UV, there was only a few ZnO formed on the galvanized steel after 1 T alternating wet/dry corrosion. The peak of ZnO increased slightly as a function of the immersion corrosion cycle. In contrast, the corrosion products of galvanized steel with UV showed significant diversity. Apart from the ZnO, $Zn_5(OH)_8Cl_2H_2O$ (Simonkolleite) appeared at approximately 10° after 1 T of corrosion, indicating a new reaction occurred under UV [29]. Meanwhile, the peak of ZnO was higher than that of the sample without UV, declaring that UV accelerates the corrosion of the zinc coating. After 25 T corrosion cycles, FeOCl, AlOCl, and $Al_2Cl_3(OH)_5{\cdot}4H_2O$ appeared, indicating that the aggressive agents penetrated the zinc coating to the Fe_2Al_5 intermetallic layer, even to the matrix [29]. SEM and XRD results further verify that UV irradiation can change the corrosion reaction on galvanized steel.

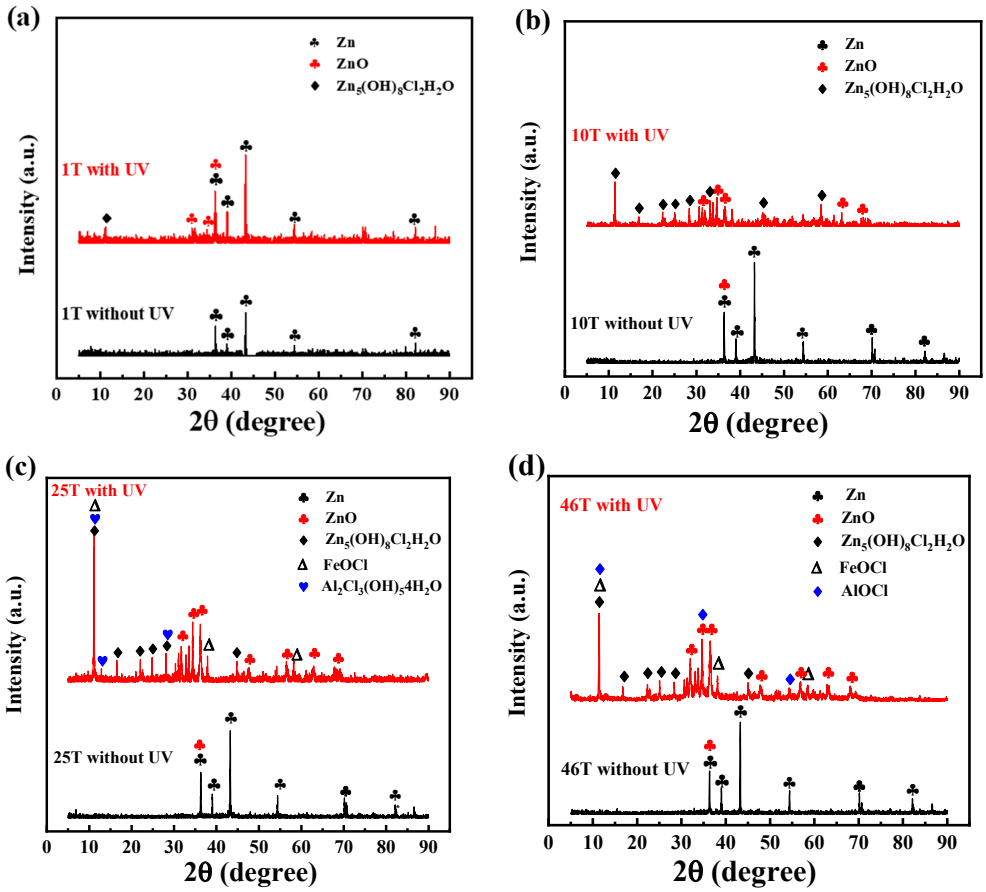


Figure 9. XRD spectrum of galvanized steel after immersion in 3.5% wt.% NaCl solution with and without UV (**a**) 1 T; (**b**) 10 T; (**c**) 25 T; and (**d**) 46 T.

3.3. Corrosion Mechanism

Based on the above results, the corrosion mechanism diagrams of galvanized steel in a simulated marine environment, under UV irradiation coupling with an alternating wet and dry in a NaCl solution, are proposed and presented in Figure 10. According to our

previous study, the galvanization process with a molten 0.1–1 at% Al-Zn bath resulted in an outer layer (Zn-Al coating), and an intermetallic film (20–50 nm) formed between the zinc coating and the steel substrate, presumably in the form of Fe_2Al_5 Zn_x ($0 < x < 1$), which can inhibit the formation of Fe-Zn intermetallic phase or "outbursts" that are detrimental to the mechanical properties of the final coating [30].

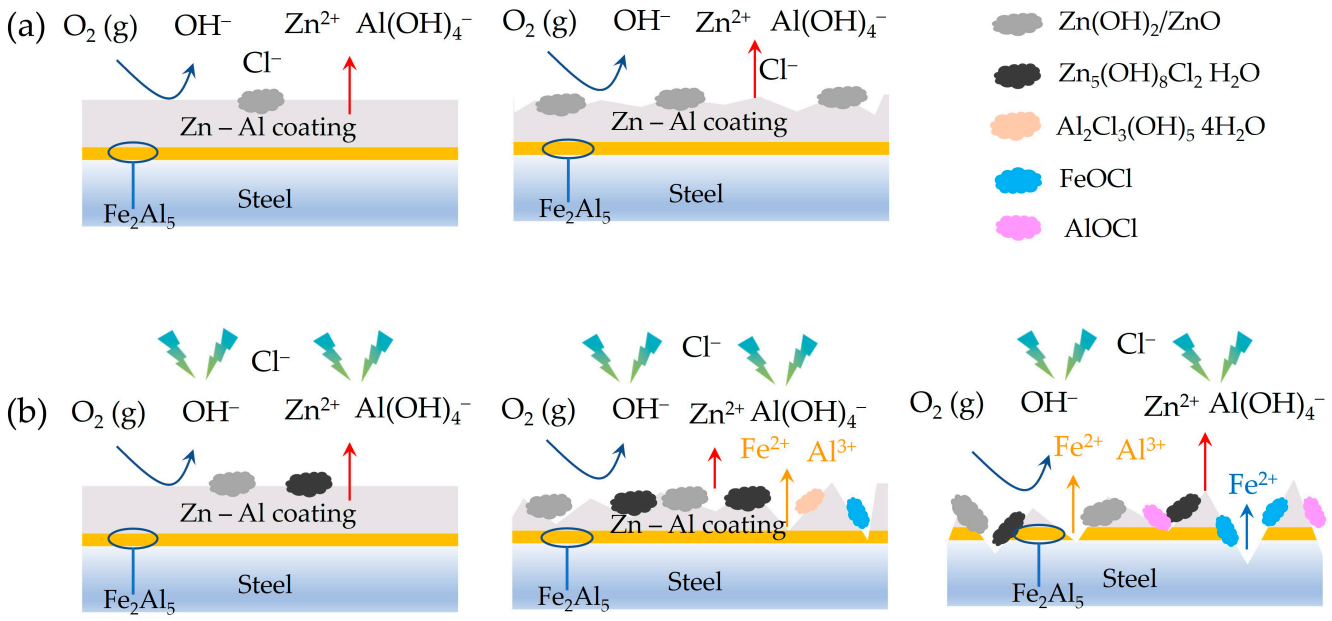


Figure 10. Corrosion mechanism of galvanized steel in an alternating wet and dry cycle NaCl solution (**a**) without UV; (**b**) with UV.

As shown in Figure 10a, in a neutral NaCl solution, the Zn-rich phase is more active than the Al-rich phase; consequently, Zn^{2+} ions formed in an anodic reaction (in Equation (1)), whilst a cathodic reaction (O_2 reduction as shown in Equation (2)) occurred on the Al-rich phase. Zn^{2+} ions reacted with the OH^- from the cathodic reaction resulting in $Zn(OH)_2$. The $Zn(OH)_2$ will transfer to ZnO because of the unstable of $Zn(OH)_2$ (Equation (3)). Meanwhile, Al will dissolve to $Al(OH)_4^-$ (Equation (4)) because of the increase in OH^- from O_2 reduction [29,31].

$$Zn \rightarrow Zn^{2+} + 2e^- \quad (1)$$

$$O_2 + 2H_2O + 4e^- \rightarrow 4OH^- \quad (2)$$

$$Zn^{2+} + 2OH^- \rightarrow Zn(OH)_2 \text{ (or } ZnO + H_2O) \quad (3)$$

$$Al + 4OH^- \rightarrow Al(OH)_4^- + 3e^- \quad (4)$$

However, under UV, the corrosion that occurs on the surface of galvanized steel is more complex and the corrosion products are numerous. According to the report, apart from ZnO, other compounds of zinc were produced on the surface of galvanized steel and the corrosion rates accelerated because of the photo-induced electrons and holes produced under UV [21]. This phenomenon was also detected in this study (Figure 9); $Zn_5(OH)_8$ Cl_2 was detected on the surface of galvanized steel under UV (Equation (5)):

$$5Zn^{2+} + 8OH^- + 2Cl^- \rightarrow Zn_5(OH)_8\ Cl_2 \quad (5)$$

With the enhancement of the corrosion reaction on the sample, Cl^- aggressively reaches the Fe_2Al_5 intermetallic film, and the intermetallic layer reacts with Cl^- to form Fe^{2+} and Al^{3+}, and then transfers to FeOCl and $Al_2Cl_3(OH)_5{\cdot}4H_2O$ or AlOCl under the UV catalytic. When the Cl^- reached the Fe matrix, the Zn-Al coating gradually lost its protective ability.

$$Fe \rightarrow Fe^{2+} + 2e^- \quad (6)$$

$$Al \rightarrow Al^{3+} + 3e^- \quad (7)$$

$$2Al^{3+} + 5OH^- + 3Cl^- + 4H_2O \rightarrow Al_2Cl_3(OH)_5{\cdot}4H_2O \quad (8)$$

$$2Fe^{2+} + O_2 + 2Cl^- \rightarrow 2FeOCl \quad (9)$$

$$2Al^{2+} + O_2 + 2Cl^- \rightarrow 2AlOCl \quad (10)$$

By the above analysis, under UV irradiation, the corrosion process of galvanized steel can be divided into three stages: (I) Zn-Al coating reacts with Cl^- aggressive agents, H_2O and O_2, to form ZnO or Zn(OH), $Zn_5(OH)_8\ Cl_2$; (II) Fe_2Al_5 intermetallic layer reacts to form FeOCl and $Al_2Cl_3(OH)_5{\cdot}4H_2O$ or AlOCl after Cl^- aggressive agents penetrate the Zn-Al coating; (III) Cl^- aggressive agents reach the steel substrate and start to dissolve. UV has an important role in atmosphere corrosion, which can accelerate the destruction of the galvanized layer on the surface of Q345B, accelerating the corrosion medium into the substrate, resulting in the destruction of the galvanized layer and a certain degree of corrosion of Q345B.

4. Conclusions

In this work, a wet/dry alternating corrosion test system coupled with UV irradiation was built to evaluate the degradation process of galvanized steel in a simulated marine atmosphere environment.

(1) The polarization and impedance results show the corrosion of galvanized steel increased as a function of the accelerating wet/dry corrosion cycles. The corrosion of galvanized steel under UV is more serious than that of galvanized steel without UV in the same corrosion cycles, which is explained by the formation of semiconductor ZnO to accelerate the corrosion process under UV.

(2) In the NaCl solution, the Zn-Al coating reacts to form ZnO and $Al(OH)_4{}^-$. The corrosion reaction gradually occurs, and corrosion products increase as a function of accelerating wet/dry corrosion cycles without UV irradiation. However, under UV irradiation, ZnO in galvanized corrosion products has semiconductor properties and the photovoltaic effect, promoting the formation of loose corrosion products $Zn(OH)_2$, $Zn_5(OH)_8\ Cl_2$, and $Al_2Cl_3(OH)_5{\cdot}4H_2O$, thus accelerating the corrosion of galvanized steel.

Supplementary Materials: The following supporting information can be downloaded at: https://www.mdpi.com/article/10.3390/cryst13081195/s1, Figure S1: (a) Photo of the galvanized steel sample; (b) Photo of the wet/dry alternating corrosion test system; Figure S2: Polarization curves of galvanized steel with and without UV after different wet and dry corrosion cycles of corrosion in 3.5% wt.% NaCl solution (a) 1 T; (b) 3 T; (c) 5 T; (d) 10 T; (e) 16 T; (f) 25 T; (g) 36 T; (h) 46 T; Figure S3: Mott-Schottky plots of galvanized steel with and without UV after different wet and dry corrosion cycles of corrosion in 3.5% wt.% NaCl solution (a) 1 T; (b) 3 T; (c) 5 T; (d) 10 T; (e) 16 T; (f) 25 T; (g) 36 T; (h) 46 T.

Author Contributions: Conceptualization, J.P. and X.L.; methodology, L.Y. and Y.W.; software, D.Y.; validation, W.L., D.Y. and C.H.; formal analysis, Y.W., B.D. and X.L.; investigation, L.Y. and Y.W.; resources, B.D. and X.L.; data curation, B.D.; writing—original draft preparation, J.P. and Y.W.; writing—review and editing, B.D. and X.L.; visualization, B.D.; supervision, X.L.; project administration, B.D. and X.L.; funding acquisition, J.P., B.D. and X.L. All authors have read and agreed to the published version of the manuscript.

Funding: This work was supported by the National Natural Science Foundation of China (No. 51901146), Key Research and Development Projects of Sichuan Provincial (2021YFG0246), and National Science and Technology Resources Investigation Program of China (Grant No. 2021FY100603).

Data Availability Statement: The raw/processed data required to reproduce these findings can be obtained through contacting the corresponding authors.

Conflicts of Interest: The authors declare no conflict of interest.

References

1. Gao, J.; Hu, W.; Wang, R.; Li, X. Study on a multifactor coupling accelerated test method for anticorrosive coatings in marine atmospheric environments. *Polym. Test.* **2021**, *100*, 107259. [CrossRef]
2. Liu, Y.; Ooi, A.; Tada, E.; Nishikata, A. Electrochemical monitoring of the degradation of galvanized steel in simulated marine atmosphere. *Corros. Sci.* **2019**, *147*, 273–282. [CrossRef]
3. Sabzi, M.; Dezfuli, S.; Asadian, M.; Tafi, A.; Mahaab, A. Study of the effect of temperature on corrosion behavior of galvanized steel in seawater environment by using potentiodynamic polarization and EIS methods. *Mater. Res. Express* **2019**, *6*, 076508. [CrossRef]
4. Vera, R.; Araya, R.; Garín, C.; Ossandón, S.; Rojas, P. Study on the effect of atmospheric corrosion on mechanical properties with impact test: Carbon steel and Galvanized steel. *Mater. Corros.* **2019**, *70*, 1151–1161. [CrossRef]
5. Liang, Y.; He, B.; Fu, G.; Wu, S.; Fan, B. Effects of ambient temperature and state of galvanized layer on corrosion of galvanized steel in high-humidity neutral atmosphere. *Materials* **2023**, *16*, 3656. [CrossRef]
6. Yang, X.; Zhang, L.; Liu, M.; Zhang, S.; Zhou, K.; She, Z.; Mu, X.; Li, D. Atmospheric corrosion behaviour of 30CrMnSiA high-strength steel in rural, industrial and marine atmosphere environments. *Corros. Eng. Sci. Technol.* **2017**, *52*, 226–235. [CrossRef]
7. Qiao, C.; Wang, M.; Hao, L.; Liu, X.; Jiang, X.; An, X.; Li, D. Temperature and NaCl deposition dependent corrosion of SAC305 solder alloy in simulated marine atmosphere. *J. Mater. Sci. Technol.* **2021**, *75*, 252–264. [CrossRef]
8. Guo, M.; Tang, J.; Pan, C.; Wang, Z. The effect of temperature and UV irradiation on corrosion behavior of 304 stainless steel exposed to a simulated marine atmosphere. *Mater. Corros.* **2022**, *73*, 876–886. [CrossRef]
9. Park, J.; Matsch, S.; Böhni, H. Effects of temperature and chloride concentration on pit initiation and early pit growth of stainless steel. *J. Electrochem. Soc.* **2002**, *149*, B34. [CrossRef]
10. Sharifi-Asla, S.; Mao, F.; Lu, P.; Kursten, B.; Macdonald, D. Exploration of the effect of chloride ion concentration and temperature on pitting corrosion of carbon steel in saturated $Ca(OH)_2$ solution. *Corros. Sci.* **2015**, *98*, 708–715. [CrossRef]
11. Wang, X.; Wang, P.; Sun, Y.; Lian, B. Corrosion resistance of Q235 steel in simulated marine atmospheric environment. *Surf. Technol.* **2015**, *44*, 104–111. [CrossRef]
12. Pan, C.; Cui, Y.; Liu, L.; Guo, M.; Wang, Z. Effect of temperature on corrosion behavior of low-alloy steel exposed to a simulated marine atmospheric environment. *J. Mater. Eng. Perform.* **2020**, *29*, 1400–1409. [CrossRef]
13. Nishikata, A.; Ichihara, Y.; Hayashi, Y.; Tsuru, T. Influence of electrolyte layer thickness and pH on the initial stage of the atmospheric corrosion of iron. *J. Electrochem. Soc.* **2014**, *161*, C288. [CrossRef]
14. Cheng, Y.; Zhang, Z.; Cao, F.; Li, J.; Zhang, J.; Wang, J.; Cao, C. A study of the corrosion of aluminum alloy 2024-T3 under thin electrolyte layers. *Corros. Sci.* **2004**, *46*, 1649–1667. [CrossRef]
15. Lin, X.; Zhang, R.; Mei, Y.; Yang, L.; Yang, F.; Dou, B.; Wei, Y. Corrosion electrochemical behavior of cadmium-plated 4340 steel in aircraft landing gear under thin electrolyte layers of potassium acetate deicing fluid. *New J. Chem.* **2019**, *43*, 14435–14442. [CrossRef]
16. Wu, J.; Wang, J. The effects of UV and visible light on the corrosion of bronze covered with an oxide film in aqueous solution. *Corros. Sci.* **2019**, *154*, 144. [CrossRef]
17. Song, L.; Chen, Z. The role of UV illumination on the NaCl-induced atmospheric corrosion of Q235 carbon steel. *Corros. Sci.* **2014**, *86*, 318–325. [CrossRef]
18. Liu, Y.; Liu, M.; Lu, X.; Wang, Z. Effect of temperature and ultraviolet radiation on corrosion behavior of carbon steel in high humidity tropical marine atmosphere. *Mater. Chem. Phys.* **2022**, *277*, 124962. [CrossRef]
19. Tatsuma, T.; Saitoh, S.; Ohko, Y.; Fujishima, A. TiO_2-WO_3 photoelectrochemical anticorrosion system with an energy storage ability. *Chem. Mater.* **2001**, *13*, 2838–2842. [CrossRef]
20. Mahmoud, M.; Wang, R.; Kato, M.; Nakasa, K. Influence of ultraviolet light irradiation on corrosion behavior of weathering steel with and without TiO_2-coating in 3 mass% NaCl solution. *Scripta. Mater.* **2005**, *53*, 1303–1308. [CrossRef]

21. Song, S.; Chen, Z. Effect of UV illumination on the NaCl-induced atmospheric corrosion of pure zinc. *J. Electrochem. Soc.* **2014**, *161*, C288. [CrossRef]
22. Abdollahi, Y.; Abdullah, A.; Zainal, Z.; Yusof, N. Photocatalytic Degradation of p-Cresol by Zinc Oxide under UV Irradiation. *Int. J. Mol. Sci.* **2012**, *13*, 302–315. [CrossRef] [PubMed]
23. Kamari, H.; Al-Hada, N.; Saion, E.; Shaari, A.; Talib, Z.; Flaifel, M.; Ahmed, A. Calcined Solution-Based PVP Influence on ZnO Semiconductor Nanoparticle Properties. *Crystals.* **2017**, *7*, 2. [CrossRef]
24. Zhang, T.; Wang, D.; Shao, Y.; Meng, G.; Wang, F. A new criterion to determine the critical pitting temperature (CPT) based on electrochemical noise measurement. *Corros. Sci.* **2012**, *58*, 202–210. [CrossRef]
25. Dou, B.; Wang, Y.; Zhang, T.; Liu, B.; Shao, Y.; Meng, G.; Wang, F. Growth behaviors of layered double hydroxide on microarc-oxidation film and anti-corrosion performances of the composite film. *J. Electrochem. Soc.* **2016**, *163*, C917–C927. [CrossRef]
26. Ge, F.; Yin, J.; Liu, Y.; Leng, W.; Wang, X.; Cui, Z. Roles of pH in the NH^{4+}-induced corrosion of AZ31 magnesium alloy in chloride environment. *J. Magnes. Alloy* **2022**, *10*, 3167–3178. [CrossRef]
27. Yang, Y.; Zhang, T.; Shao, Y.; Meng, G.; Wang, F. In situ study of dew point corrosion by electrochemical measurement. *Corros. Sci.* **2013**, *71*, 62–71. [CrossRef]
28. Cui, Z.; Li, X.; Xiao, K.; Dong, C. Atmospheric corrosion of field-exposed AZ31 magnesium in a tropical marine environment. *Corros. Sci.* **2013**, *76*, 243–256. [CrossRef]
29. Azevedo, M.; Allély, C.; Ogle, K.; Volovitch, P. Corrosion mechanisms of Zn(Mg, Al) coated steel in accelerated tests and natural exposure: 1. The role of electrolyte composition in the nature of corrosion products and relative corrosion rate. *Corros. Sci.* **2015**, *90*, 472–481. [CrossRef]
30. Dou, B.; Li, X.; Han, J.; Ogle, K. Operando kinetics of hydrogen evolution and elemental dissolution I: The dissolution stoichiometry of galvanized steel in hydrochloric acid. *Corros. Sci.* **2023**, *214*, 111007. [CrossRef]
31. Mokaddem, T.; Volovitch, P.; Ogle, K. The anodic dissolution of zinc and zinc alloys in alkaline solution. II. Al and Zn partial dissolution from 5% Al–Zn coatings. *Electrochim. Acta* **2012**, *74*, 130–138. [CrossRef]

Disclaimer/Publisher's Note: The statements, opinions and data contained in all publications are solely those of the individual author(s) and contributor(s) and not of MDPI and/or the editor(s). MDPI and/or the editor(s) disclaim responsibility for any injury to people or property resulting from any ideas, methods, instructions or products referred to in the content.